PERSPECTIVE

Molecular catalysis science: Perspective on unifying the fields of catalysis

Rong Ye[a,b], Tyler J. Hurlburt[a,b], Kairat Sabyrov[a,b], Selim Alayoglu[b], and Gabor A. Somorjai[a,b,1]

Edited by Mark E. Davis, California Institute of Technology, Pasadena, CA, and approved March 28, 2016 (received for review February 1, 2016)

Colloidal chemistry is used to control the size, shape, morphology, and composition of metal nanoparticles. Model catalysts as such are applied to catalytic transformations in the three types of catalysts: heterogeneous, homogeneous, and enzymatic. Real-time dynamics of oxidation state, coordination, and bonding of nanoparticle catalysts are put under the microscope using surface techniques such as sum-frequency generation vibrational spectroscopy and ambient pressure X-ray photoelectron spectroscopy under catalytically relevant conditions. It was demonstrated that catalytic behavior and trends are strongly tied to oxidation state, the coordination number and crystallographic orientation of metal sites, and bonding and orientation of surface adsorbates. It was also found that catalytic performance can be tuned by carefully designing and fabricating catalysts from the bottom up. Homogeneous and heterogeneous catalysts, and likely enzymes, behave similarly at the molecular level. Unifying the fields of catalysis is the key to achieving the goal of 100% selectivity in catalysis.

catalysis | surface chemistry | nanocatalyst synthesis | in situ characterization | real-time dynamics

Two major breakthroughs have revolutionized molecular catalysis science over the last 20 y. The first is in the development of nanomaterials science (1–4), which has made it possible to synthesize metallic (5–7), bimetallic, and core-shell nanoparticles (8, 9), mesoporous metal oxides (10, 11), and enzymes (12–16) in the nanocatalytic range between 0.8 and 10 nm. The second innovation is in the advancement of spectroscopy and microscopy instruments (17–20)—including nonlinear laser optics (21), sum-frequency generation vibrational spectroscopy (22–24), and synchrotron-based instruments, such as ambient pressure X-ray photoelectron spectroscopy (8, 25–27), X-ray absorption near-edge structure, extended X-ray absorption fine structure (28–30), infrared (IR) and X-ray microspectroscopies (31), and high-pressure scanning tunneling microscopies (32, 33)—that characterize catalysts at the atomic and molecular levels under reaction conditions (34). Most of the studies that use these techniques focus on nanoscale technologies, such as catalytic energy conversion and information storage, which have reduced the size of transistors to below 25 nm (35).

Catalysts are classified into three types—heterogeneous, homogeneous, and enzymatic—and, in most cases, range in size from 1 to 10 nm, which is even smaller than the transistors being developed by the latest size-fabrication technologies. Heterogeneous catalysts work in reaction systems with multiple phases (e.g., solid-gas or solid-liquid phase); homogeneous catalysts reside in the same phase as the reactants, almost always in the liquid phase; and enzymatic catalysts, which are most active in an aqueous solution, make use of active sites in proteins. The catalysis of chemical energy conversion provides ever-increasing selectivity in producing combustible hydrocarbons, gasoline, and diesel.

The tenets that direct our catalysis research involve nanoparticle synthesis, characterization under reaction conditions, and reaction studies using these nanoparticles to determine kinetics, selectivity, deactivation, and other catalytic kinetic parameters. These variables are studied in the same research group because they are the underpinning of molecular catalysis. The hypothesis that we are striving to support is that the three fields of catalysis (heterogeneous, homogeneous, and enzyme) behave similarly on the molecular level. These ongoing studies as well as their success and future outlook are the subjects of this paper.

[a]Department of Chemistry, University of California, Berkeley, CA 94720; and [b]Chemical Sciences Division, Lawrence Berkeley National Laboratory, Berkeley, CA 94720

Author contributions: G.A.S. designed research; R.Y., T.J.H., K.S., and S.A. performed research; and R.Y., T.J.H., K.S., S.A., and G.A.S. wrote the paper.

The authors declare no conflict of interest.

This article is a PNAS Direct Submission.

[1]To whom correspondence should be addressed. Email: somorjai@berkeley.edu.

Metal Nanoparticles for Size-Dependent Covalent Bond Catalysis

The major technique for the synthesis of nanoparticle catalysts is colloid chemistry (Fig. 1*A*). These nanoparticle-based catalysts are produced with precisely controlled sizes in the 1- to 10-nm range in two dimensions using the Langmuir–Blodgett technique (36) or placed on porous 3D supports. The nanoparticles, mostly metals, are placed in a microporous and mesoporous support. The mesoporous support is made with mesoporous silica between 5- and 25-nm pores coated by a transition metal oxide. The silica is removed by leaching with sodium hydroxide to leave behind a mesoporous template that is loaded up with nanoparticles used for catalytic studies. The oxide itself, as it will be shown, is often a very important ingredient for catalytic reactions (34).

In our work, we found that the size and shape of metal nanoparticles control both catalytic reaction rates and selectivities. We also learned that all of these multipath reactions show size dependence in their turnover rates and selectivity (37). It is possible to achieve different shapes of platinum nanoparticles (Fig. 1*B*), and the size regime of platinum nanoparticles can be sharply focused in the 1.5- to 8.0-nm range (Fig. 1*C*). Such a well-defined particle size and distribution are essential to detecting the turnover rates of the hydrogenation of either benzene or toluene because they are structure-sensitive. We also observed fourfold change in turnover rates between nanoparticles of platinum in the 2- to 4-nm range and in the 4- to 6-nm range. The size and shape dependence of nanoparticles can readily be controlled by colloid science technology (36, 38, 39) (Fig. 1*C*). The isomerization of methylcyclopentane is much more shape-dependent on the platinum nanoparticles than size-dependent (40) (Fig. 2*A*). In the case of the Fischer–Tropsch CO hydrogenation reaction, the product distribution is size-dependent (41), and the turnover rate increases fivefold with increasing size (Fig. 2*B*).

Characterization Under Reaction Conditions

Previous studies examined catalysts only before use (i.e., as-made or prenatal catalysts) and after use (i.e., spent or postmortem catalysts) and thus could not determine how a metal nanocatalyst's structure and other properties, including composition and oxidation states, would change as a function of reaction time, temperature, and pressure.

Engineering chemical and physical properties at molecular levels is a challenging task that requires tools and strategies, known as in situ probing, to characterize catalysts in action. This in situ method measures macroscopic and microscopic properties simultaneously or separately under identical or similar conditions in an attempt to correlate function and structure (31). In addition to this in situ approach, surface techniques—with temporal, spatial, and chemical resolutions in their respective scales of subsecond, subnanometer, and vibrational and electronic levels—are prerequisites to gaining molecular insight into catalysts' operations (42–44). These techniques are often based on detecting outbound electrons, photons, or ions of catalysts of interest upon excitation with high-energy electrons or photons in a broad

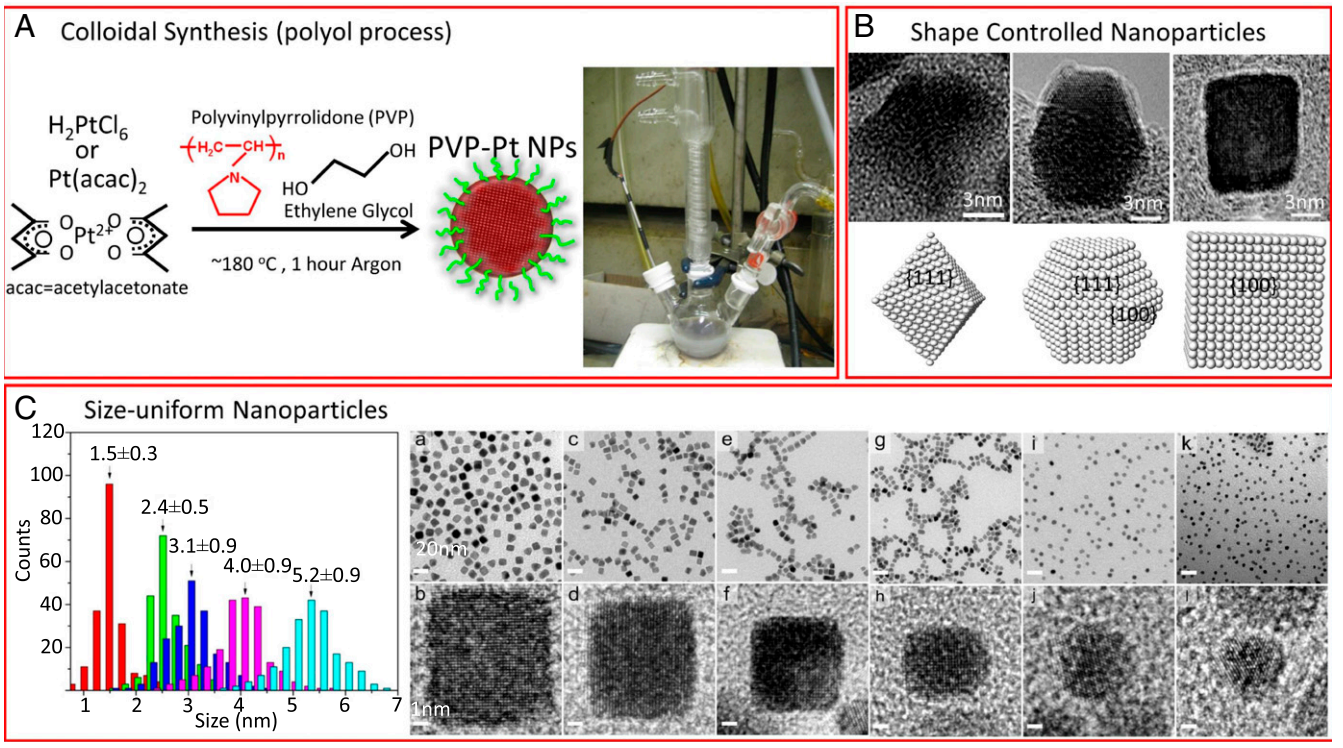

Fig. 1. Examples of size and shape control of nanoparticles. (*A*) Schematic of Pt nanoparticles synthesis by the polyol reduction method. (*B*) Transmission electron microscopy (TEM) images and ball models of Pt nanoparticles with different shapes. (*C*, *Left*) Particle size distribution histograms of the Pt/SBA-15 series catalysts obtained from TEM images. The number inserts indicate the mean particle diameter and SD for each sample. (*Right*) TEM and high-resolution TEM (HRTEM) images of Pt nanocrystals with different shapes and sizes. TEM images of (*a*) 9-nm nanocubes, (*c*) 7-nm nanocubes, (*e*) 6-nm nanocubes, (*g*) 5-nm nanocubes, (*i*) 5-nm nanopolyhedra, and (*k*) 3.5-nm nuclei. HRTEM images of a single (*b*) 9-nm nanocube, (*d*) 7-nm nanocube, (*f*) 6-nm nanocube, and (*h*) 5-nm nanocube along the [100] zone axis. HRTEM images of a single (*j*) 5-nm nanopolyhedron, and (*l*) 3.5-nm nucleus along the [111] zone axis. (Scale bars: Tem images, 20 nm; HRTEM images, 1 nm.) Panels adapted with permission as follows: *B*, ref. 36, American Chemical Society; *C*, *Left*, ref. 38, Elsevier; *C*, *Right*, ref. 39, American Chemical Society.

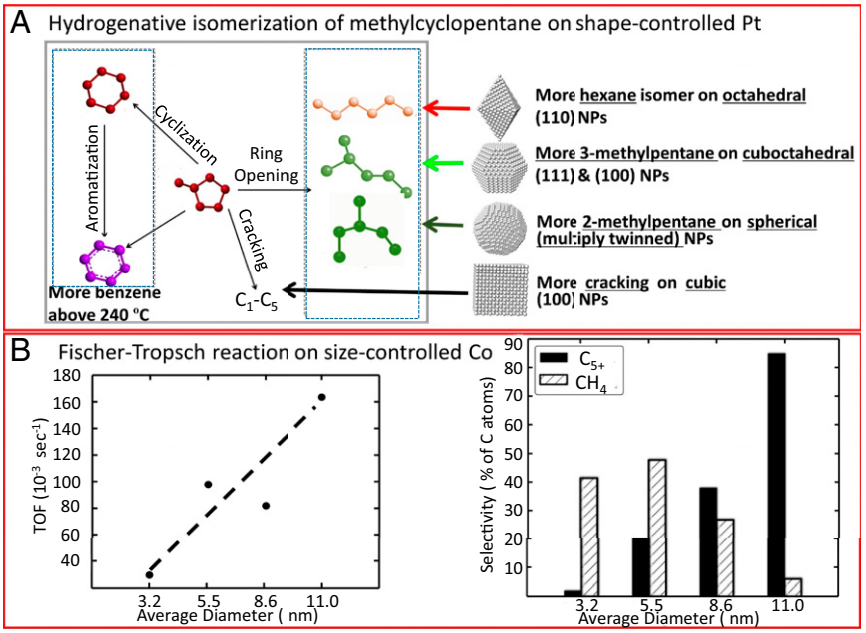

Fig. 2. Examples of shape and size dependence of nanoparticle catalysts. (*A*) Reaction pathways and possible products of methylcyclopentane hydrogenation reaction catalyzed by Pt nanoparticles with different shapes. (*B*, *Left*) CO consumption turnover frequency for the CO hydrogenation at 5 bar (H_2:CO = 2:1) for various sizes of cobalt nanoparticle catalysts supported on MCF-17. The turnover frequency (TOF) corresponds to the number of CO molecules converted in time divided by the number of cobalt atoms at the catalyst surface. (*Right*) Selectivities toward hydrocarbons with a carbon number of 5 and higher (C_{5+}) and methane selectivities (SCH_4) as a function of cobalt crystallite sizes for hydrogenation of carbon monoxide (H_2:CO = 2:1) at 5 bar and 250 °C. Both selectivities are expressed relative to the total number of carbon atoms converted. Panels adapted with permission as follows: *A*, ref. 40, Springer; *B*, ref. 41, Springer.

electromagnetic spectrum, ranging from radio waves to IR and visible light and to UV and X-rays. Monochromated in energies and collimated or focused in space, these probes carry electronic, vibrational, and bonding information, giving away fundamental details of the otherwise hidden components of a catalyst—pieces of a puzzle and snapshots of a bigger picture.

Fig. 3*A* shows sum-frequency generation nonlinear optical spectroscopy (24), which is very sensitive to the surface-adsorbed species under catalytic reaction conditions (22–24, 45). Several molecular species are found (23) on the surface during ethylene hydrogenation, cyclohexene hydrogenation, and dehydrogenation (Fig. 3*B*). Although some species, as well as their turnover rates,

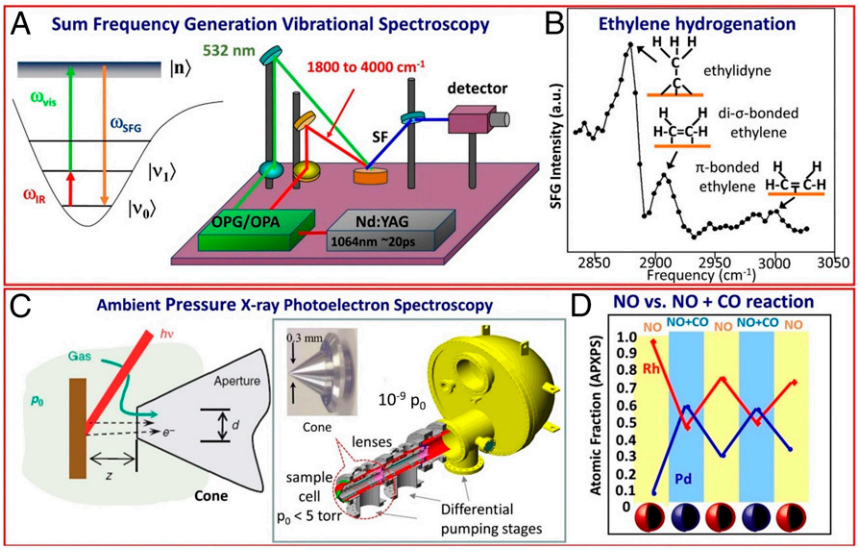

Fig. 3. In situ characterization of catalyst surfaces using sum-frequency generation (SFG) and XPS. (*A*) Schematic of a high-pressure SFG system, a vibrational spectroscopic tool for probing the adsorbed species during the catalytic reaction. (*B*) SFG spectra of adsorbed species on Pt (111) during ethylene hydrogenation under 35 torr of ethylene, 100 torr of H_2, and 625 torr of He. (*C*) Schematic of ambient pressure XPS setup at Beamline 9.3.2 of the Advanced Light Source at Lawrence Berkeley National Laboratory. (*D*) Evolution of Rh (Rh^0 + Rh^{2+}) and Pd (Pd^0 + Pd^{2+}) atomic fractions in the $Rh_{0.5}Pd_{0.5}$ NPs at 300 °C under oxidizing conditions (100 mtorr NO or O_2) and catalytic conditions (100 mtorr NO and 100 mtorr CO) denoted in the *x* axis. APXPS, ambient-pressure X-ray photoelectron spectroscopy; NP, nanoparticles. Panels adapted with permission as follows: *A*, ref. 25, American Chemical Society; *B*, ref. 23, Elsevier; *C*, ref. 27; *D*, ref. 8, AAAS.

change dynamically under these conditions, others are merely spectators. The mechanistic details are revealed by sum-frequency generation under reaction conditions.

Ambient pressure X-ray photoelectron spectroscopy (XPS) is shown (8, 25–27) schematically in Fig. 3*C*. Bimetallic nanoparticles are shown being studied by this technique. Palladium-rhodium bimetallic nanoparticles 15 nm in size show rhodium segregation under nitric oxide (NO) adsorption-induced oxidizing conditions. Palladium catches up with rhodium surface composition when we add a reducing gas—carbon monoxide (CO)—adsorbed on the surface (8). The outcome of these studies is to show that bimetallic nanoparticles undergo a surface composition change that is driven by dynamic chemical oxidizing and reducing environments (Fig. 3*D*).

A high-pressure scanning tunneling microscope (STM) (32, 33) shows that the adsorbates reacting on the catalyst surface are mobile under reaction conditions. For example, when cyclohexene hydrogenation and dehydrogenation turnovers are measured under reaction conditions, the STM image is diffused. This observation indicates that the adsorbate molecules move at a faster rate than the scanning tunneling tip's surface motion of 100 Å/ms. However, if the surface is contaminated by carbon monoxide adsorption, cyclohexene hydrogenation and dehydrogenation reaction turnovers come to a halt, and an ordered surface structure forms, which is readily detectable by STM. We observed that not only are the adsorbed molecules mobile under catalytic reaction conditions, but the adsorbate-induced restructuring of the metal surfaces is also enhanced by high reactant pressures. The stepped platinum single crystal surfaces became clustered and rearranged at high-pressure carbon monoxide adsorption (Fig. 4*A*). This clustered formation is reversible, however: when carbon monoxide is removed from the surface by evacuation (33), the stepped structure of the original crystal surface is reestablished.

Oxidation State of Nanoparticles Changes with Decreasing Size: Conversion of Heterogeneous to Homogeneous Catalysis

When CO oxidation was studied on rhodium nanoparticle surfaces as a function of size below 2 nm, the CO oxidation rates increased by 30-fold. Ambient pressure XPS studies (46) indicated that the higher turnover rates are due to the oxidation state of rhodium changing from metallic rhodium to rhodium^{3+} (Fig. 4*B*). Similar studies on platinum indicated that platinum nanoparticles above 1.5 nm are metallic; however, the studies also found that platinum below 1.5 nm and as low as 0.8 nm are in the 2^+ and 4^+ oxidation states (29, 47). Because very few bulk atoms are available for these nanoparticles, they become dominated by low coordination surface atoms, and, as a result, their electronic structure changes. Nørskov and coworkers (48) have studied this process and found that the adsorption energy of oxygen on gold

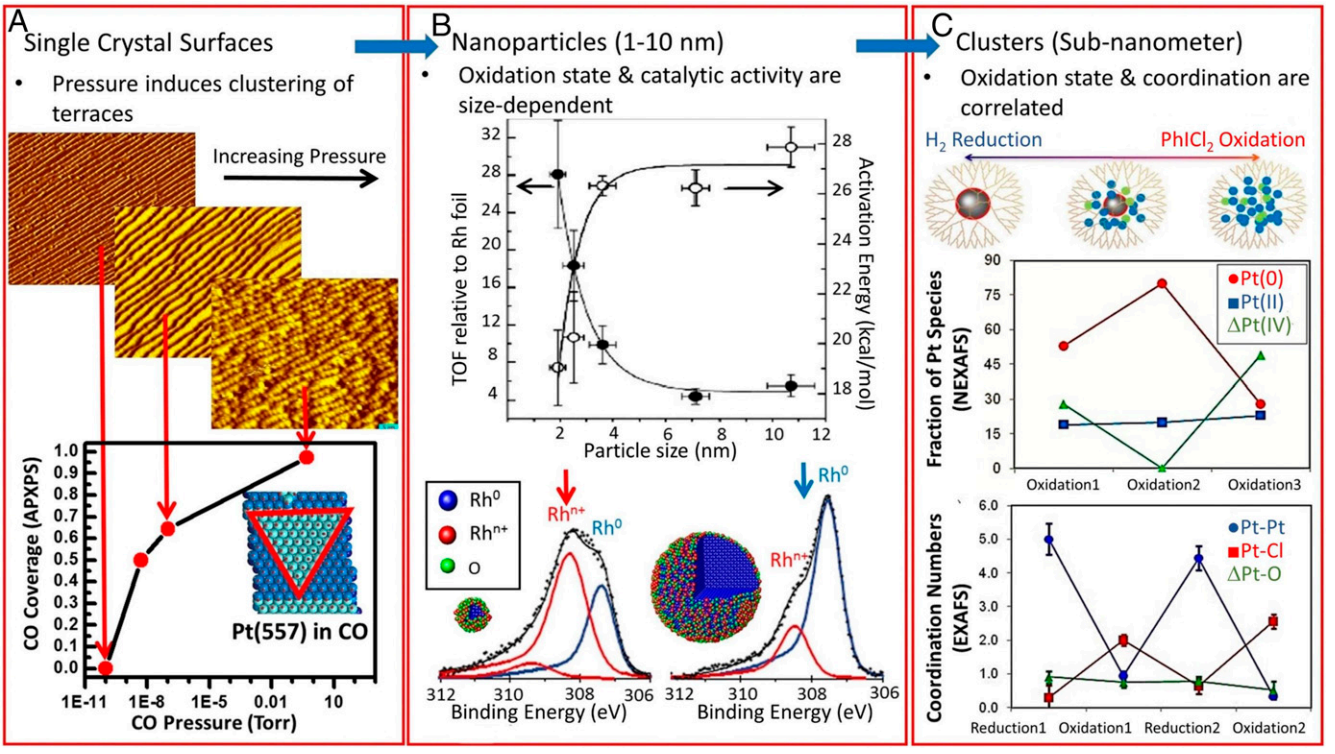

Fig. 4. In situ characterization of catalysts in decreasing sizes using STM, XPS, near-edge X-ray absorption fine structure (NEXAFS), and EXAFS. (*A*) STM images of Pt(557) in increasing pressure of CO from 1×10^{-10} torr to 1 torr and the corresponding CO coverage determined by APXPS. STM images are 40 nm by 50 nm in size. (*B*) Turnover frequency relative to rhodium foil at 50 torr O_2, 20 torr CO, at 200 °C, and activation energy (150–225 °C) for CO oxidation. APXPS data show the difference of oxidation state of nanoparticles with 2 nm diameter and 11 nm diameter. (*C*, *Top*) A scheme based on the X-ray absorption spectroscopy (XAS) results, showing possible structures of the dendrimer-encapsulated Pt catalyst after reduction and oxidation treatment. The gray spheres represent the metallic Pt clusters. The surface Pt chlorides are indicated by red circles. The small blue and green species represent the Pt(II) and Pt(IV) species formed after oxidation treatment. (*Middle*) The fractions of Pt(0) and Pt(II) and Pt(IV) chloride species of the Pt catalyst derived from NEXAFS analysis. (*Bottom*) Average coordination numbers of Pt atoms in the supported Pt catalyst after a sequence of hydrogen reduction and $PhICl_2$ oxidation treatments in the toluene derived from EXAFS analysis. Panels adapted with permission as follows: *A*, ref. 33, AAAS; *B*, ref. 46; *C*, ref. 29, American Chemical Society.

nanoparticles changes as a function of a decrease in size. Because there is a decrease in the gold coordination number at the adsorption sites and fewer than 55 atoms, which is slightly more than 1 nm, the gold becomes oxidized to gold 1^+ and 3^+ instead of metallic gold.

The homogeneous catalysts are usually single transition metal ions, surrounded by ligands. As a result, we tried to use these small nanoclusters, which have controlled high oxidation states, to carry out homogeneous catalysis. We adsorbed the small nanoclusters on dendrimers, tree-like polymers that hold these nanoparticles throughout its branches. We found that these dendrimer-encapsulated nanoparticles are excellent homogeneous catalysts so we managed to heterogenize homogeneous catalysts by using nanoparticles composed of 40 atoms of rhodium, palladium, gold, or platinum for reactions including hydroformylation, decarbonylation, and other commonly known homogeneous catalytic reactions (3, 31, 47, 49–53). We demonstrated that catalytic reactivity and selectivity could be tuned by changing the dendrimer properties, in a similar fashion to ligand modification in an organometallic homogeneous catalyst (51, 53). X-ray absorption spectroscopy studies [X-ray absorption near edge structure (XANES) and extended X-ray absorption fine structure (EXAFS)] showed (28–30) that the nanoparticles dispersed to small low coordination clusters under oxidizing conditions but reassembled to the original 1-nm particles when under reduction by reactants, products, or the dendrimers (Fig. 4*C*). This process is also reversible.

Likewise, single site homogeneous catalysts are low coordination systems comprised of ligands that control electronic structure and chemistry at the molecular level (29, 54). By controlling types and binding of ligands, a high level of selectivity (regio- and enantio-selectivity) is obtained in homogenized catalytic reactions. Capping agents used in colloidal synthesis, similar to ligands in single site organometallic complexes, can be used to control selectivity in heterogenized homogeneous reactions, which, as of today, remains a great challenge.

Oxide–Metal Interfaces as Active Sites for Acid–Base Catalysis

Platinum is an excellent hydrogenation catalyst of many organic molecules, such as crotonaldehyde. When platinum nanoparticles of the same size are placed on two different oxides—silica and titania—one can see that the turnover rates and the selectivities are much higher when titania rather than silica is used as a support. The importance of the oxide support for metal catalysts to change selectivities and product distributions is well-known. This phenomenon of the oxide support effect on catalytic reaction rates, where the oxide alone does not carry out the same or any reaction, is called positive strong metal support interaction (SMSI) in the literature (55). It is the charge transfer ability of reducible oxide supports that acts on the performance of metal catalysts: But how does charge regulate catalytic processes?

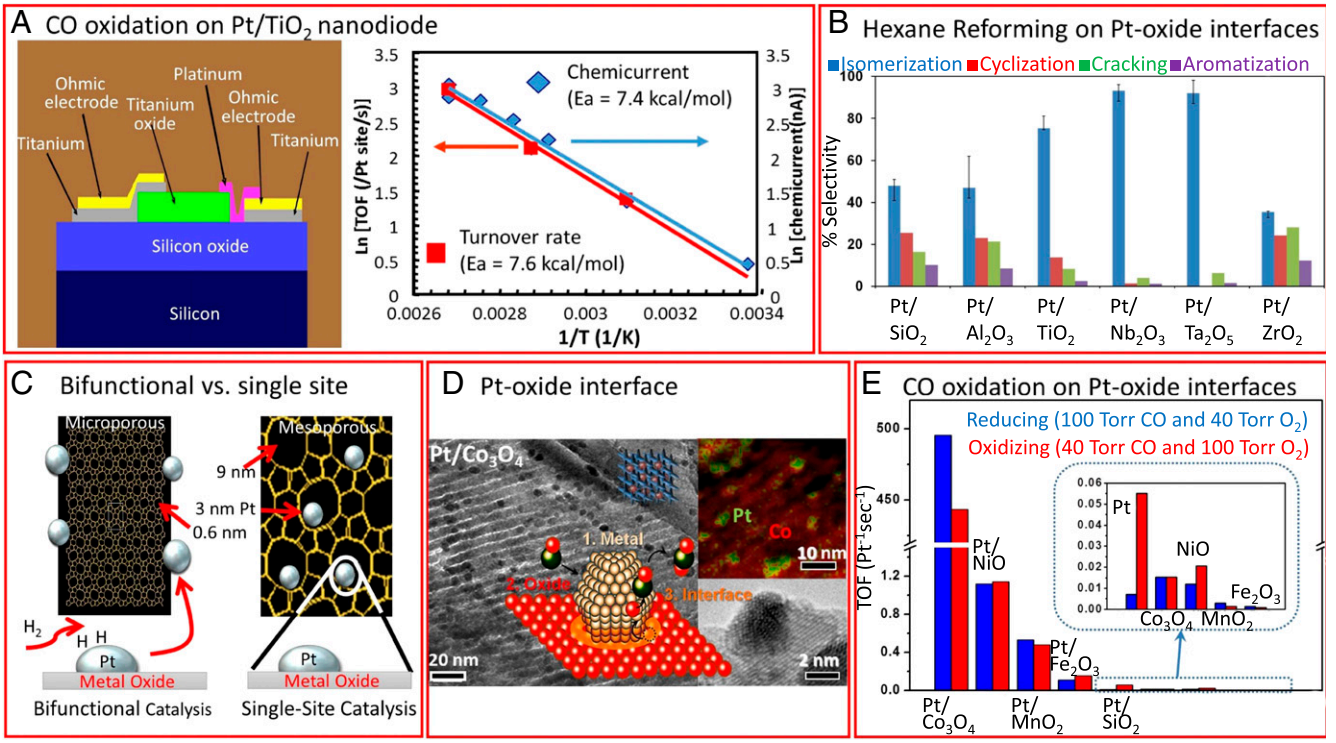

Fig. 5. Evidence for the importance of the metal oxide support on catalysis. (*A*, *Left*) Schematic of Pt/TiO_2 device. (*Right*) Arrhenius plots obtained from chemicurrent and turnover measurements on a Pt/TiO_2 diode with pressure of 6 torr of H_2 and 760 torr O_2. Both give similar activation energies, which implies that hot electron generation under hydrogen oxidation is proportional to the catalytic turnover rate. (*B*) Product distributions of *n*-hexane isomerization over 2.7 nm Pt nanoparticle catalysts supported on different kinds of oxide supports at 360 °C. (*C*) Schematics of the differences between bifunctional and single-site catalysis. (*D*, *Left*) TEM image of Pt/Co_3O_4 catalysts. (*Top Right*) Energy-dispersive spectroscopy (EDS) phase mapping of Pt/Co_3O_4 catalysts, showing the merged image of the Co K (red) and Pt L (green) lines. (*Bottom Right*) High-resolution TEM image of Pt/Co_3O_4 catalysts. (*Inset Top*) Illustration of mesoporous-oxide-supported Pt nanoparticle catalysts. (*Inset Bottom*) An illustration showing the potential reaction sites of Pt-nanoparticle-loaded oxide catalysts during CO oxidation. (*E*) Comparison of TOFs at 473 K of CO oxidation over Pt-nanoparticle-loaded oxide and pure mesoporous oxide catalysts. Panels adapted with permission as follows: *A*, *Left*, ref. 56, American Vacuum Society; *A*, *Right*, ref. 58, American Chemical Society; *B*, ref. 59, American Chemical Society; *D* and *E*, ref. 60, American Chemical Society.

An explanation was found by surface physics studies of hot electron emission under light illumination that was carried out by exothermic catalytic reactions on metal surfaces (56), such as CO oxidation or hydrogen oxidation (Fig. 5*A*). The deposited energy produces high kinetic energy electrons that have a mean free path within the metal in the range of 5–10 nm. The chemical energy deposition in metals to produce hot electrons has been well demonstrated by Huang et al. (57) using highly vibrationally excited NO molecules impinging on gold compared with lithium fluoride surfaces. On gold, the NO molecules in the 15th vibrationally excited state lose 1.5 eV of energy to produce molecules in the eighth vibrational state. On the other hand, the vibrationally excited NO molecules lost no energy when they scattered from lithium fluoride, which has no free electrons. The hot electron generation can be observed by using exothermic catalytic reactions on a Schottky diode on platinum and titanium oxide where the platinum is less than about 5 nm in thickness. The charge flow between the platinum and the titanium oxide allows one to determine the current flow in the battery configuration shown in Fig. 5*A*. One can detect a so-called chemicurrent, which is correlated with the turnover rate of exothermic CO oxidation or hydrogen oxidation reactions (58). Theoretical calculations showed that the transition state in these processes involves CO_2^- or H_2O^-, which yields the chemicurrent that is proportional to the turnover rate. In this study, acid–base catalysis is correlated with charge concentration, and not with surface area. On the other hand, covalent bond catalysis is known to be surface area-dependent. These two modes of catalysis are the major ways chemistry occurs in most catalytic processes.

When one places metal nanoparticles into a mesoporous oxide support, many oxide–metal interfaces are produced within the mesopores between the metal and the oxide. Studies have found that these oxide–metal interfaces have major effects on catalytic reactions. The isomerization of *n*-hexane on naked oxide only results in the cracking of the *n*-hexane molecules whereas mesoporous oxides give rise to 100% selectivity of *n*-hexane isomers of high octane numbers (59) in the presence of platinum (Fig. 5*B*). Fig. 5 *C*–*E* shows similar effects when platinum is placed on various oxide mesopores. Platinum nanoparticles produce very little CO oxidation within mesoporous silica, but, when they are placed on mesoporous cobalt oxide, more than a 1,000-fold increase in catalytic turnover for CO oxidation kinetics is found.

Fig. 5*C*, *Right* shows mesoporous transition metal oxide-supported platinum nanoparticles. This image is the oxide–metal interface, which produces large, strong metal support effects. There is a charge transfer between the metal and the oxide under reaction conditions. If the oxide is alone, as in the case of *n*-hexane conversion with pure oxides of niobium oxide, titanium oxide, and other oxides, only the cracking of the *n*-hexane molecules is observed. However, if the platinum is in the mesopores, a 100% selectivity to isomerization is produced, which is very high and an important factor in making high-octane gasoline.

Fig. 5*C*, *Left* shows platinum nanoparticles in contact with microporous oxides when the platinum nanoparticle is much larger and cannot fit into the micropores. In this case, the chemistry that occurs—known as bifunctional catalysis—is the sum total of the chemistry of platinum and the microporous oxide, which act in parallel or consecutively. In the other case, when the mesoporous transition metal oxide can accommodate the 3-nm platinum inside its mesopores, there are oxide–metal interfaces, where charge transfer and acid–base catalysis occur, which are uniquely selective in many circumstances. Similar results are seen when CO oxidation is carried out on platinum supported by silica or another transition metal oxide (60). The turnover rate on silica is small, equal to pure platinum turnover; however, when cobalt oxide is the mesoporous support, the turnover rate is amplified by a 1,000-fold (Fig. 5*E*). This finding is indeed a major increase in catalytic activity.

Hybrid Systems: Outlook

It is clear that we can heterogenize homogeneous catalysts. However, enzymes (12–16) are also very important catalytic systems, and recent studies have focused on how to synthesize pure enzymes as well as on how to look for similarities between enzymes and all three catalytic systems on the molecular scale. For example, it is known that, when enzymes are immobilized on a surface, they gain the reusability and ease of separation seen in heterogeneous catalysts, as well as in some cases becoming more stable to wider pH and temperature ranges (61–63). It is planned to advance previous work by immobilizing enzymes on a solid surface and studying the enzyme–solid interface at the molecular level, and to

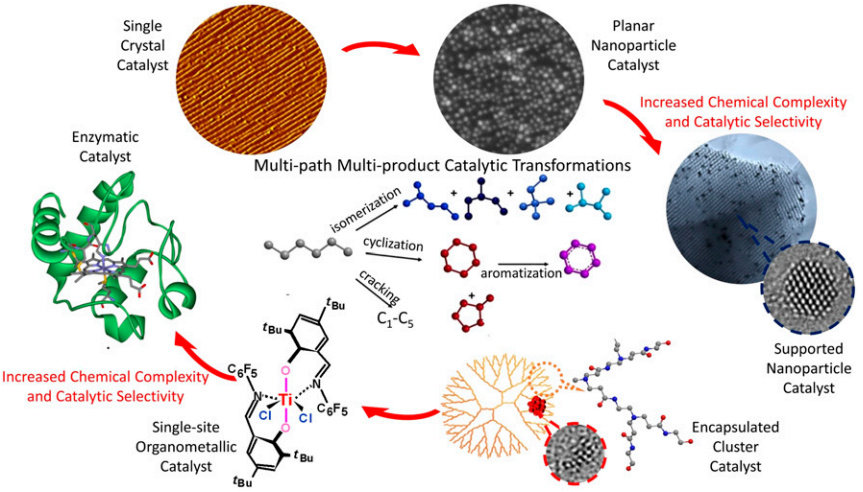

Fig. 6. Schematics showing the evolution of catalyst complexity leading to increased catalytic selectivity for multipath and multiproduct catalytic transformations. Enzymatic catalyst adapted with permission from ref. 14, AAAS.

develop a molecular understanding of all three types of catalysts under similar conditions of reactions and chemical environments.

In our attempt to focus on the chemical correlations between the three catalysis groups—heterogeneous, homogeneous, and enzymatic—the future looks very promising for molecular catalysis science studies. Catalysis of homogeneous, heterogeneous, or enzymatic origin alike involve nano-sized materials. These nanocatalysts comprise inorganic and/or organic components. Charge, coordination, interatomic distance, bonding, and orientation of catalytically active atoms are molecular factors shared by all three fields of catalysis. By controlling the governing catalytic components and molecular factors, catalytic processes of a multichannel and multiproduct nature could be run in all three catalytic platforms to create unique end products. Fig. 6 illustrates the promise of a molecularly unified catalytic scheme of the future.

Acknowledgments

The work shown in this perspective article was supported by the Director, Office of Science, Office of Basic Energy Sciences, Chemical Sciences, Geosciences and Biosciences Division of the US Department of Energy under Contract De-AC02-05CH11231.

1 Batista CA, Larson RG, Kotov NA (2015) Nonadditivity of nanoparticle interactions. *Science* 350(6257):1242477.
2 Yin Y, Alivisatos AP (2005) Colloidal nanocrystal synthesis and the organic-inorganic interface. *Nature* 437(7059):664–670.
3 Crooks RM, Zhao M, Sun L, Chechik V, Yeung LK (2001) Dendrimer-encapsulated metal nanoparticles: Synthesis, characterization, and applications to catalysis. *Acc Chem Res* 34(3):181–190.
4 Li H, Eddaoudi M, O'Keeffe M, Yaghi OM (1999) Design and synthesis of an exceptionally stable and highly porous metal-organic framework. *Nature* 402(6759): 276–279.
5 Schrinner M, et al. (2009) Single nanocrystals of platinum prepared by partial dissolution of Au-Pt nanoalloys. *Science* 323(5914):617–620.
6 Lee I, Morales R, Albiter MA, Zaera F (2008) Synthesis of heterogeneous catalysts with well shaped platinum particles to control reaction selectivity. *Proc Natl Acad Sci USA* 105(40):15241–15246.
7 Sun Y, Xia Y (2002) Shape-controlled synthesis of gold and silver nanoparticles. *Science* 298(5601):2176–2179.
8 Tao F, et al. (2008) Reaction-driven restructuring of Rh-Pd and Pt-Pd core-shell nanoparticles. *Science* 322(5903):932–934.
9 Stamenkovic VR, et al. (2007) Improved oxygen reduction activity on Pt3Ni(111) via increased surface site availability. *Science* 315(5811):493–497.
10 Yang P, Zhao D, Margolese DI, Chmelka BF, Stucky GD (1998) Generalized syntheses of large-pore mesoporous metal oxides with semicrystalline frameworks. *Nature* 396(6707):152–155.
11 Zhao D, et al. (1998) Triblock copolymer syntheses of mesoporous silica with periodic 50 to 300 angstrom pores. *Science* 279(5350):548–552.
12 Glowacki DR, Harvey JN, Mulholland AJ (2012) Taking Ockham's razor to enzyme dynamics and catalysis. *Nat Chem* 4(3):169–176.
13 Hay S, Scrutton NS (2012) Good vibrations in enzyme-catalysed reactions. *Nat Chem* 4(3):161–168.
14 Bhabha G, et al. (2011) A dynamic knockout reveals that conformational fluctuations influence the chemical step of enzyme catalysis. *Science* 332(6026):234–238.
15 Boehr DD, McElheny D, Dyson HJ, Wright PE (2006) The dynamic energy landscape of dihydrofolate reductase catalysis. *Science* 313(5793):1638–1642.
16 Nureki O, et al. (1998) Enzyme structure with two catalytic sites for double-sieve selection of substrate. *Science* 280(5363):578–582.
17 Liao H-G, et al. (2014) Nanoparticle growth: Facet development during platinum nanocube growth. *Science* 345(6199):916–919.
18 de Oteyza DG, et al. (2013) Direct imaging of covalent bond structure in single-molecule chemical reactions. *Science* 340(6139):1434–1437.
19 Bao W, et al. (2012) Mapping local charge recombination heterogeneity by multidimensional nanospectroscopic imaging. *Science* 338(6112):1317–1321.
20 Choi JS, et al. (2011) Friction anisotropy-driven domain imaging on exfoliated monolayer graphene. *Science* 333(6042):607–610.
21 Umstadter D, Chen S, Maksimchuk A, Mourou G, Wagner R (1996) Nonlinear optics in relativistic plasmas and laser wake field acceleration of electrons. *Science* 273(5274):472–475.
22 Holinga GJ, et al. (2011) An SFG study of interfacial amino acids at the hydrophilic SiO2 and hydrophobic deuterated polystyrene surfaces. *J Am Chem Soc* 133(16):6243–6253.
23 McCrea KR, Somorjai GA (2000) SFG-surface vibrational spectroscopy studies of structure sensitivity and insensitivity in catalytic reactions: Cyclohexene dehydrogenation and ethylene hydrogenation on Pt (1 1 1) and Pt (1 0 0) crystal surfaces. *J Mol Catal Chem* 163(1–2):43–53.
24 Shen Y (1989) Surface properties probed by second-harmonic and sum-frequency generation. *Nature* 337:519–525.
25 Alayoglu S, et al. (2012) In situ surface and reaction probe studies with model nanoparticle catalysts. *ACS Catal* 2(11):2250–2258.
26 Salmeron M, Schlögl R (2008) Ambient pressure photoelectron spectroscopy: A new tool for surface science and nanotechnology. *Surf Sci Rep* 63(4):169–199.
27 Bluhm H, et al. (2007) In situ X-ray photoelectron spectroscopy studies of gas-solid interfaces at near-ambient conditions. *MRS Bull* 32(12):1022–1030.
28 Velasco-Velez J-J, et al. (2014) Interfacial water: The structure of interfacial water on gold electrodes studied by x-ray absorption spectroscopy. *Science* 346(6211): 831–834.
29 Li Y, et al. (2011) A Pt-cluster-based heterogeneous catalyst for homogeneous catalytic reactions: X-ray absorption spectroscopy and reaction kinetic studies of their activity and stability against leaching. *J Am Chem Soc* 133(34):13527–13533.
30 Jiao F, Frei H (2009) Nanostructured cobalt oxide clusters in mesoporous silica as efficient oxygen-evolving catalysts. *Angew Chem Int Ed Engl* 48(10):1841–1844.
31 Gross E, et al. (2014) In situ IR and X-ray high spatial-resolution microspectroscopy measurements of multistep organic transformation in flow microreactor catalyzed by Au nanoclusters. *J Am Chem Soc* 136(9):3624–3629.
32 Zhu Z, et al. (2013) Structure and chemical state of the Pt(557) surface during hydrogen oxidation reaction studied by in situ scanning tunneling microscopy and X-ray photoelectron spectroscopy. *J Am Chem Soc* 135(34):12560–12563.
33 Tao F, et al. (2010) Break-up of stepped platinum catalyst surfaces by high CO coverage. *Science* 327(5967):850–853.
34 Somorjai GA, Li Y (2010) *Introduction to Surface Chemistry and Catalysis* (Wiley, Hoboken, NJ), 2nd Ed.
35 Franklin AD (2015) Device Technology. Nanomaterials in transistors: From high-performance to thin-film applications. *Science* 349(6249):aab2750.
36 Song H, Kim F, Connor S, Somorjai GA, Yang P (2005) Pt nanocrystals: Shape control and Langmuir-Blodgett monolayer formation. *J Phys Chem B* 109(1): 188–193.
37 Lee I, Delbecq F, Morales R, Albiter MA, Zaera F (2009) Tuning selectivity in catalysis by controlling particle shape. *Nat Mater* 8(2):132–138.
38 Pushkarev VV, An K, Alayoglu S, Beaumont SK, Somorjai GA (2012) Hydrogenation of benzene and toluene over size controlled Pt/SBA-15 catalysts: Elucidation of the Pt particle size effect on reaction kinetics. *J Catal* 292:64–72.
39 Tsung C-K, et al. (2009) Sub-10 nm platinum nanocrystals with size and shape control: Catalytic study for ethylene and pyrrole hydrogenation. *J Am Chem Soc* 131(16):5816–5822.
40 Alayoglu S, Aliaga C, Sprung C, Somorjai GA (2011) Size and shape dependence on Pt nanoparticles for the methylcyclopentane/hydrogen ring opening/ring enlargement reaction. *Catal Lett* 141(7):914–924.
41 Melaet G, Lindeman A, Somorjai G (2014) Cobalt particle size effects in the Fischer–Tropsch synthesis and in the hydrogenation of CO2 studied with nanoparticle model catalysts on silica. *Top Catal* 57(6-9):500–507.
42 Buurmans ILC, Weckhuysen BM (2012) Heterogeneities of individual catalyst particles in space and time as monitored by spectroscopy. *Nat Chem* 4(11):873–886.

43 van Schrojenstein Lantman EM, Deckert-Gaudig T, Mank AJG, Deckert V, Weckhuysen BM (2012) Catalytic processes monitored at the nanoscale with tip-enhanced Raman spectroscopy. *Nat Nanotechnol* 7(9):583–586.
44 de Smit E, et al. (2008) Nanoscale chemical imaging of a working catalyst by scanning transmission X-ray microscopy. *Nature* 456(7219):222–225.
45 Somorjai GA, Frei H, Park JY (2009) Advancing the frontiers in nanocatalysis, biointerfaces, and renewable energy conversion by innovations of surface techniques. *J Am Chem Soc* 131(46):16589–16605.
46 Grass ME, et al. (2008) A reactive oxide overlayer on rhodium nanoparticles during CO oxidation and its size dependence studied by in situ ambient-pressure X-ray photoelectron spectroscopy. *Angew Chem Int Ed Engl* 47(46):8893–8896.
47 Crooks RM, Zhao M (1999) Dendrimer-encapsulated Pt nanoparticles: Synthesis, characterization, and applications to catalysis. *Adv Mater* 11(3):217–220.
48 Kleis J, et al. (2011) Finite size effects in chemical bonding: From small clusters to solids. *Catal Lett* 141(8):1067–1071.
49 Huang W, et al. (2008) Dendrimer templated synthesis of one nanometer Rh and Pt particles supported on mesoporous silica: Catalytic activity for ethylene and pyrrole hydrogenation. *Nano Lett* 8(7):2027–2034.
50 Witham CA, et al. (2010) Converting homogeneous to heterogeneous in electrophilic catalysis using monodisperse metal nanoparticles. *Nat Chem* 2(1):36–41.
51 Gross E, Liu JH-C, Toste FD, Somorjai GA (2012) Control of selectivity in heterogeneous catalysis by tuning nanoparticle properties and reactor residence time. *Nat Chem* 4(11):947–952.
52 Huang W, et al. (2010) Highly active heterogeneous palladium nanoparticle catalysts for homogeneous electrophilic reactions in solution and the utilization of a continuous flow reactor. *J Am Chem Soc* 132(47):16771–16773.
53 Gross E, et al. (2013) Asymmetric catalysis at the mesoscale: Gold nanoclusters embedded in chiral self-assembled monolayer as heterogeneous catalyst for asymmetric reactions. *J Am Chem Soc* 135(10):3881–3886.
54 Oliver-Meseguer J, Cabrero-Antonino JR, Domínguez I, Leyva-Pérez A, Corma A (2012) Small gold clusters formed in solution give reaction turnover numbers of 10(7) at room temperature. *Science* 338(6113):1452–1455.
55 Tauster SJ, Fung SC, Baker RTK, Horsley JA (1981) Strong interactions in supported-metal catalysts. *Science* 211(4487):1121–1125.
56 Park JY, Somorjai GA (2006) Energy conversion from catalytic reaction to hot electron current with metal-semiconductor Schottky nanodiodes. *J Vac Sci Technol B* 24(4):1967–1971.
57 Huang Y, Rettner CT, Auerbach DJ, Wodtke AM (2000) Vibrational promotion of electron transfer. *Science* 290(5489):111–114.
58 Hervier A, Renzas JR, Park JY, Somorjai GA (2009) Hydrogen oxidation-driven hot electron flow detected by catalytic nanodiodes. *Nano Lett* 9(11):3930–3933.
59 An K, Alayoglu S, Musselwhite N, Na K, Somorjai GA (2014) Designed catalysts from Pt nanoparticles supported on macroporous oxides for selective isomerization of n-hexane. *J Am Chem Soc* 136(19):6830–6833.
60 An K, et al. (2013) Enhanced CO oxidation rates at the interface of mesoporous oxides and Pt nanoparticles. *J Am Chem Soc* 135(44):16689–16696.
61 Torres-Salas P, et al. (2011) Immobilized biocatalysts: Novel approaches and tools for binding enzymes to supports. *Adv Mater* 23(44):5275–5282.
62 Matosevic S, Szita N, Baganz F (2011) Fundamentals and applications of immobilized microfluidic enzymatic reactors. *J Chem Technol Biotechnol* 86(3):325–334.
63 Roessl U, Nahálka J, Nidetzky B (2010) Carrier-free immobilized enzymes for biocatalysis. *Biotechnol Lett* 32(3):341–350.